Desalination and Water Treatment
www.deswater.com

doi: 10.5004/dwt.2021.27711

236 (2021) 190–202
October

Characterization of activated carbon prepared from date palm fibers by physical activation for the removal of phenol from aqueous solutions

Djehad Bentarfa[a], Mohamed L. Sekirifa[a], Mahfoud Hadj-Mahammed[a], Dominique Richard[b], Stephanie Pallier[b], Bachari Khaldoun[c], Hakim Belkhalfa[c], Ammar H. Al-Dujaili[d,*]

[a]*Laboratoire de Biogéochimie en Milieux Désertiques, Faculté des Mathématiques et des Sciences de la Matière, Université Kasdi Merbah, Ouargla, Algeria, Tel. +213-698324257; email: djehadbentarfa@gmail.com (D. Bentarfa), Tel. +213-6-62122572; email: smedlamine@gmail.com (M.L. Sekirifa), Tel. +231-771779351; email: hadjmahf@yahoo.fr (M. Hadj-Mahammed)*
[b]*Laboratoire de Génie des Procédés Catalytiques-LGPC-CNRS/CPE Lyon, Villeurbanne cedex, France, Tel. +33615388455; email: dri@lgpc.cpe.fr (D. Richard), Tel. +33472431760; email: ras@lgpc.cpe.fr (S. Pallier)*
[c]*Scientific and Technical Research Center in Physico-Chimical Analysis, Algeria, Tel. +213662778515; email: bachari2000@yahoo.fr (B. Khaldoun), Tel. +213 662778415; email: hakimbelkhalfa@gmail.com (H. Belkhalfa)*
[d]*Hamdi Mango Center for Scientific Research, University of Jordan, Amman, P.O. Box 11942, Jordan, Tel. +962 796 629 774; email: ah.aldujaili@gmail.com (A.H. Al-Dujaili)*

Received 8 April 2021; Accepted 9 August 2021

ABSTRACT

This study investigated the alternative cheap eco-friendly materials date palm (*Phoenix dactylifera*) fibers for the preparation of activated carbon (AC) by physical activation with CO_2 at different parameters of pyrolysis: pyrolysis temperature, the particle size and the duration of pyrolysis. The physical characterization (porosity and surface) was determined by the adsorption–desorption of nitrogen at 77 K (BET) and Dubinin–Radushkevich (D-R) equations, as well as the analysis by scanning electron microscopy. The chemical characterization (surface function), which was carried out by the Boehm titration, the pH zero-point charge (pH_{zpc}) and Fourier transform infrared spectroscopy, confirmed the acidic character of the material. The adsorption of phenol from aqueous solutions onto the prepared AC was investigated. The adsorption process followed the Langmuir isotherm model with a maximum adsorption capacity of 31.75 mg g^{-1} for date palm fibers.

Keywords: AC of date palm fibers; Activated carbon; Physical activation; Adsorption; Isotherm; Phenol

1. Introduction

Owing to their harmfulness to life types, even at low concentrations, phenolic compounds are listed as priority contaminants. Phenol has been registered by the U.S. Environmental Protection Agency (USEPA) as a hazardous contaminant with a permissible restriction of 0.1 mg L^{-1} in wastewater, it is necessary to remove it from wastewater before it is released into wastewater for the protection of public water and health [1,2]. Several methods, including chemical oxidation, photo-catalytic degradation, ultrasonic degradation, solvent extraction and adsorption, have been produced to remove phenol from waste water. Overall, the safest method is still the adsorption process [3].

* Corresponding author.

Due to its effectiveness, economy, high capacity to separate an outsized scope of product mixtures, adsorption is better than the alternative separation techniques [4,5], and its simple methodology utilizing various adsorbents such as activated carbon [6–8], alumina [8], silica gel [8] and zeolites [9]. It is widely agreed that ACs (granular or powdered) have a highly defined pore structure, one of the most frequently used as adsorbents, catalysts [10,11], electrode materials of super capacitors [12], and catalyst support for the removal of pollutant species from gases or liquids and for purification or recovery of chemicals due to their excellent adsorption capability for inorganic pollutants [6]. In the previous few years, research has been centered on the use of waste materials from agricultural products because they are cheap, rational and eco-friendly to manufacture adsorbents, the properties of ACs are dependent on the activation process and hence the nature of the source [13]. Several materials such as wood wastes [14], coffee residue [15], slash pine bark [16], apricot stones [17], date stones [18,19], date pits [20,21], date palm trunk fiber [22] and olive stones [23] have been used for preparation of AC. AC preparations typically include two steps, primarily the process of pyrolysis and activation [24], chemical activation by the use of dehydrating agents such as H_2SO_4, H_3PO_4, KOH and $ZnCl_2$. Physical activation using carbon dioxide (CO_2), steam or a combination of both [25,26]. CO_2 was chosen as the activation gas in the current work: CO_2 is spotless and easy to deal with. In addition, CO_2 has been a favored decision as to the activation gas on the laboratory scale: it facilitates control of the activation process [27,28].

The number of date palms (*Phoenix dactylifera*) in the world is estimated at almost 100 million palm trees, with 32.5 million date palms in second position in Africa. With more than 20 million date palm trees in total, Algeria is one of the leading countries in the cultivation and processing of palm dates in Africa and the Arab world, becoming the fourth largest date producer in the world, and its production is concentrated in the southeastern part of the country; Biskra, El Oued and Ouargla [29,30].

A large number of by-products, such as leaves, petioles, rachis, trunk leaflets, are produced as mentioned in the date palm tree. Products obtained from bunches (fruit bunch branch of palm, date seeds) without proper use (as a residue) because they are mostly disposed of by burning or are regarded as animal feed or waste and have rarely been used in crafts, such as basketry, crates, ropes, and traditional construction [29]. So we have an approximate amount of date palm (*Phoenix dactylifera*) fibers, although considered to be the world's leading accessible fiber types, these amounts are likely to be of interest in promoting commercial sustainability through the development of alternative cheap eco-friendly materials [31].

In the marketing of date palm type (Ghars), the state of Ouargla ranks first [32]. That is why, in our current research, we decided to invest date palm fibers as raw materials to prepare AC by physical activation with CO_2 at different conditions of impact, such as pyrolysis temperature, particle size and pyrolysis length.

The aim of the present study is to characterize and verify the effectiveness of AC, using several methods such as: the adsorption-desorption of nitrogen at 77 K (BET), using D-R equations, analysis by scanning electron microscopy (SEM), Boehm titration method, the pH_{zpc}, Fourier transform infrared spectroscopy (FTIR), and characterization of adsorption capacity by adsorption of phenol using UV-Vis spectroscopy.

2. Materials and methods

2.1. Adsorbent preparation

Palm waste, namely Ghars (Fig. 1) date palm fiber, was collected from a date palm oasis in Ouargla, Algeria. To extract all dirt and dust at their initial particle size, the fibers were washed with distilled water, followed by filtration and then dried at room temperature. They were then crushed and sieved after drying. The fractions between two sets (250 μm < d < 500 μm) and (45 μm < d < 125 μm) was named RF_1 and RF_2, respectively.

The pyrolysis was carried out at 500°C for 2 h under a 250 mL min^{-1} nitrogen flow and a heating rate of 5°C min^{-1} using a vertical furnace (Ref. BGVA12-300B, CARBOLITE), 75 g of crushed date palm fibers were added in a 40-mm internal diameter cylindrical quartz cell including a half-height frit dish. At 600°C for 2 h, the resulting pyrolysis date palm fibers were triggered. The carbon dioxide flow rate was maintained at 250 mL min^{-1} and heating rate of 5°C min^{-1}. The pyrolysis and activation conditions of the samples are shown in Table 1.

2.2. Physical characterization

The pore structures of the resulting ACs were analyzed using N_2 adsorption and SEM.

Table 1
Pyrolysis and activation conditions of the RF_1 and RF_2 raw materials

			Pyrolysis condition		
Raw materials	Granulation	Sample	Temperature and duration	Flow and heating rate	Activation condition
RF_1	(250 μm < D < 500 μm)	ACF_1	600°C, 2 h	250 mL min^{-1} (N_2), 5°C min^{-1}	600°C, 2 h, 250 mL min^{-1} (CO_2), 5°C min^{-1}.
		ACF_2	500°C, 2 h		
		ACF_3	500°C, 1 h		
RF_2	(45 μm < D < 125 μm)	ACF_4	500°C, 2 h		
		ACF_5	500°C, 3 h		

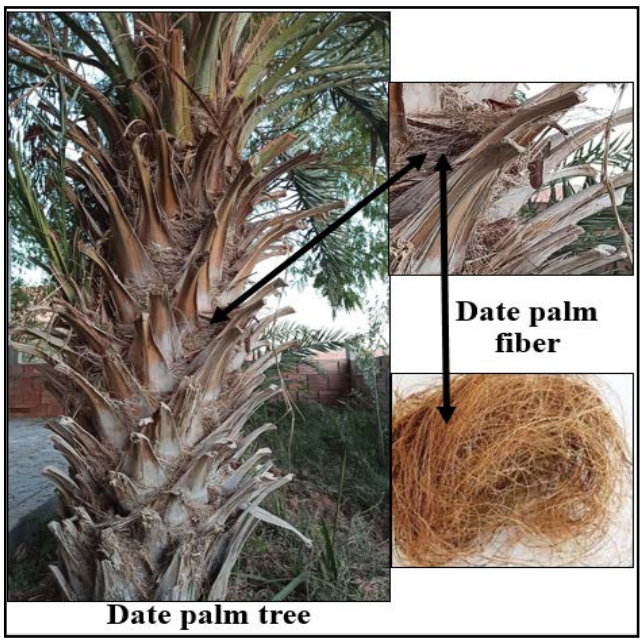

Fig. 1. Date palm tree and date palm fibers Ghars.

2.2.1. N_2 adsorption

N_2 adsorption–desorption isothermal measurements at liquid nitrogen temperature (77 K) using ASAP 2010 characterized the textural heterogeneity of the prepared ACs (Micromeritics Instrument Company, Norcross/USA). By using the BET method [33], the BET specific surface areas (S_{BET}) were measured, assuming that the surface area occupied by the nitrogen molecule was 0.162 nm^2. On the basis of the liquid volume of nitrogen adsorbed at a relative pressure of p/p_o = 0.97, the total pore volume (V_{tot}) was calculated. According to IUPAC classification [34], the size of the micropores L (nm) (pores < 2 nm) was calculated according to the D-R equation [35]. The microporous surface (S_{micro}) and external surface (S_{ext}) as well as the volume of micropores (V_{mic}) were assessed by the *t*-plot method [36]. The mesopore volume (V_{mes}) was obtained by deducting the micropore volume from the total pore volume. The average pore diameters (D_p) were estimated from the S_{BET} and V_{tot} assuming an open-ended cylindrical pore model without pore networks [37].

2.2.2. Scanning electron microscopy

The micrographs were obtained with a SEM (EVO ZEISS 15) equipped with a secondary electron detector (SE1). Micrographs were obtained under an acceleration voltage of 20 kV with a 1.00 K magnification to estimate the surface pore structure of the ACs.

2.3. Surface chemistry characterization

There are a range of techniques for the characterization of ACs in surface chemistry to qualitatively and quantitatively classify their surface functional groups [38,39]. We use the pH_{zpc}, which displays the charge on AC surfaces. The characterization of the AC by Boehm titration by surface chemistry (acidity-basicity) is useful for testing its surface charge and acidity, and FTIR to classify functional groups in ACs.

The pH of the AC samples was determined according to the ASTM D6851 method by mixing AC with deionized water with the pH measured by the pH meter after 1 d at 25°C.

The pH value required to give zero net surface charge (zero electric charge) is a convenient measure of the tendency of the AC surface to become either positively or negatively charged as a function of pH [40,41]. This value is designated as the point of zero charge of AC samples (zpc) (pH_{zpc}), this method was conducted to determine the pH_{zpc} of AC of date palm fiber, and it was measured as follows: 2 L of 0.1 N NaCl was prepared and divided into 40 flasks each one containing 50 mL solutions. Then, their pH values were adjusted between 2 and 12 with the addition of 0.1 N solution of HCl or NaOH. pH of initial solutions was measured with a pH meter and then noted as $pH_{initial}$. After the constant value of $pH_{initial}$ had been reached, 0.15 g of AC sample was added into each flask and then shaken for 5 d at 25°C. After 5 d, pH of the solution was measured and noted as pH_{final}. Thus, the curve $pH_i - pH_f = f(pH_i)$ was drawn. The point of intersection between this curve and the line of equation $x = 0$ gives the pH at the zero point charges of the active carbon considered.

2.4. Study of surface functions

To determine the composition of active carbon in terms of acidic or basic surface groups, the Boehm method was used (Boehm 1966). Using 0.1 N of $NaHCO_3$, Na_2CO_3 and NaOH, the acidic groups were found. As well as to neutralize the basic groups, a 0.1 N HCl was used [36]. For each sample, a mass of 0.5 g is added to a 25 mL of solutions prepared into a series of flasks at 25°C for 72 h. After filtration, the solutions are then dosed with HCl or NaOH at a concentration of 0.1 N in the presence of phenolphthalein as an indicator. $NaHCO_3$ neutralizes the carboxylic groups (–COOH), Na_2CO_3 neutralizes the carboxylic groups (–COOH) and the lactone groups (–COO–) and NaOH neutralizes the carboxylic groups (–COOH), lactone (–COO–) and phenolic groups (–OH). The number of functional groups of the various acid functions is calculated by considering that $NaHCO_3$ neutralizes the carboxylic groups (–COOH). Based on the above method, the different acidic groups can be determined [37].

2.5. Infrared spectroscopy

The chemical structures of ACs were analyzed by attenuated total reflection-Fourier transform infrared (ATR-FTIR) spectrometer using Cary 600 series FTIR spectrometer (Santa Clara, California). The analysis was performed in a transmittance mode, the functional groups in the ACs in the range of 4,000–600 cm^{-1} can be identified [25,39].

2.6. Characterization of adsorption capacity of phenol

Immersion calorimetry is the method based on the selective adsorption of the phenol from dilute aqueous solutions to ACs [40].

2.7. Adsorbate preparation

A 1,000-mg L^{-1} of stock solution was prepared by dissolving 0.5 g of the solid phenol powder into 500 mL of deionized water. All working solutions were prepared by diluting the stock solution with deionized water.

2.8. Adsorption procedure

In order to determine the phenol adsorption potential of ACF samples at 25°C, phenol adsorption measurements were carried out by measuring the UV-Vis absorption intensity for a series of phenol stock solutions with known concentrations at λ_{max} = 270 nm using a spectrophotometer, a calibration curve was recorded (Cary Series UV-Vis spectrophotometer). About 40 mg of each ACF samples were added into test tubes containing 10 mL of stock solution with five different concentrations (20–100 mg L^{-1}). All the test tubes were shaken for 3 h using (Bench Mixer Multi-Tube Vortexer) to ensure even mixing of the ACF with the target phenol solution. About 5 mL of phenol solution was taken using a filtered syringe. Then, the phenol solution was scanned by UV-Vis spectrophotometer. The concentrations of phenol solutions were obtained by comparing the absorbance intensity to the calibration curve. The amount of phenol adsorbed at equilibrium q_e (mg g^{-1}) was calculated by the following equation:

$$q_e = \frac{\left(C_o - C_e\right)V}{m} \tag{1}$$

where C_o and C_e are the liquid-phase concentrations (mg L^{-1}) of phenol at initial and at equilibrium, respectively. V is the volume (L) of the solution and m is the mass (g) of dry adsorbent used.

The percentage of phenol removal (%R) is defined as the ratio between the difference between the phenol concentration before and after adsorption (C_o – C_e) and the initial aqueous solution phenol concentration (C_o) and was calculated using an equation.

$$\%R = \frac{C_o - C_e}{C_0} \times 100\% \tag{2}$$

2.9. Isotherm studies

The relationship between adsorbate molecules and adsorbent surface isotherms can be defined by adsorption isotherms [42]. To balance the experimental results, two types of isothermal models (Langmuir and Freundlich) were tested.

The linear form of Langmuir isotherm is represented as follows [43]:

$$\frac{C_e}{q_e} = \frac{1}{K_L q_{\max}} + \frac{C_e}{q_{\max}} \tag{3}$$

where q_e is the amount of phenol adsorbed per unit mass of the adsorbent at equilibrium (mg g^{-1}), q_{max} is the maximum adsorption capacity of the adsorbent (mg g^{-1}) and K_L is the Langmuir equilibrium constant related to the affinity of binding sites and energy of adsorption (L mg^{-1}).

The essential characteristics of the Langmuir isotherm can be expressed, according to Al-Haidary et al. [44], in terms of the separation factor or equilibrium parameter R_L that can be determined from the relationship (Eq. (4)), which is indicative of the isotherm form that predicts whether an adsorption mechanism is favorable or unfavorable. R_L is characterized as follows:

$$R_L = \frac{1}{1 + K_L C_o} \tag{4}$$

where C_o is the highest initial concentration (mg L^{-1}). R_L was also determined to know the feasibility of the isotherm. Values of the R_L express the type of isotherm to be either unfavorable ($R_L > 1$), linear ($R_L = 1$), favorable ($1 > R_L > 0$), or irreversible ($R_L = 0$).

The linear equation of Freundlich isotherm is given by Freundlich as follows [43]:

$$\mathrm{Log}\, q_e = \mathrm{Log}\, K_F + \frac{1}{n}\mathrm{Log}\, C_e \tag{5}$$

where K_F is the Freundlich constant that is related to bond strength [(mg g^{-1}) (L $mg^{-1})^{1/n}$]; n is the Freundlich constant and indicative of bond energies.

2.10. Statistical evaluation

The accuracy of the equilibrium and kinetic models was evaluated from the chi-square (χ^2), coefficient of determination values (R^2). The χ^2 and R^2 were calculated according to Eqs. (6) and (7) [45].

$$\chi^2 = \sum \frac{\left(q_{e,\exp} - q_{e,\mathrm{cal}}\right)^2}{q_{e,\mathrm{cal}}} \tag{6}$$

$$R^2 = \frac{\sum\left(q_{e,\mathrm{cal}} - q_{e,\mathrm{mean}}\right)^2}{\sum\left(q_{e,\mathrm{cal}} - q_{e,\mathrm{mean}}\right)^2 + \sum\left(q_{e,\mathrm{cal}} - q_{e,\exp}\right)^2} \tag{7}$$

Langmuir and Freundlich isotherm models were also tested using an error function ($F_{error\%}$) [46], which measures the variations in the quantity of phenol taken up by the adsorbent predicted by the models and the real q_e measured experimentally.

$$F_{\mathrm{error}\%} = 100 \times \sqrt{\sum_i^N \left[\frac{q_{e,\exp} - q_{e,\mathrm{cal}}}{q_{e,\exp}}\right]^2 / \left(N - P\right)} \tag{8}$$

where $q_{e,exp}$ (mg/g) is the equilibrium quantity of phenols extracted from Eq. (1), $q_{e,cal}$ (mg/g) is the quantity of phenols extracted from the models and $q_{e,mean}$ (mg/g) is the mean of $q_{e,exp}$ values, N is the number of experimental information points, P is the number of model parameters.

3. Results and discussion

3.1. Burn-off of AC fiber

To determine the effect of activation period on pore growth, the burn-off for the ACF derived from date palm fiber Ghars was analyzed. Based on the following equation, the burn-off of ACF was calculated:

$$\text{Burn-off}(\%) = \frac{m_i - m_f}{m_i} \times 100\% \quad (9)$$

where m_i and m_f are the initial and final mass (g) of ACF, respectively. It can be seen from Table 2 that the burn-off for ACF_1, ACF_2, ACF_3, ACF_4 and ACF_5 samples are 82.38, 95.73, 93.7, 93.54 and 92.96 wt %, respectively. With the decrease in pyrolysis temperature from 600°C for ACF_1 to 500°C for ACF_2, the burn-off increased from 82.38 to 95.73 wt%. The values of burn-off for ACF_3, ACF_4 and ACF_5 decreased from 93.7 to 93.54 and 92.96 wt %, respectively, as duration time increased from 1 to 3 h. In addition, the values of burn-off of ACF_2 and ACF_4 decreased from 95.73 to 93.54 wt %, respectively, as the granularity decrease from (250 μm < D < 500 μm) to (45 μm < D < 125 μm). These results suggested that the lower the temperature and duration of pyrolysis and the larger the sample size, the burn-off increases. The rise in burn-off suggested the elimination of more volatile organic species that eventually improved the ACF's pore growth. Porosity enhancement may increase the surface area of the ACF and thus affect the ability of adsorption. It is apparent that despite lower yield, high burn-off is the vital aim to produce highly porous ACF for the effective adsorption process [47].

3.2. Characterization methods

In order to achieve the best characteristics for the Ghars date palm fibers, the AC samples were prepared under optimized conditions described in our previous work [18]. In order to determine the degree of its effect, the optimized conditions for CO_2 activation are the activation temperature and time of 600°C and 2 h, respectively, and the CO_2 flow and heating rate of 250 mL min^{-1} and 5°C min^{-1}, respectively, with the change in the pyrolysis conditions.

To characterize the pore structure of the ACF samples, the N_2 adsorption–desorption isotherms obtained with the different ACs in the 77 K experiment were performed, as shown in Figs. 2 and 3 situations with distinct results. These figures show the effect of the temperature of the pyrolysis, the effect of the size of the particles and the effect of the duration time of the pyrolysis on the adsorbed quantity, respectively. We note that the rise in the volume of adsorbed nitrogen is related to the decrease in temperature of the pyrolysis, the increase in size of the particle and increase in the duration of the pyrolysis; since through the figures we find that the lower the temperature of the pyrolysis, the longer the duration of the pyrolysis, and the larger the size of the particle, the greater the amount of N_2 adsorbed.

Dense micropore structures (dimensions < 2 nm) belonging to the type I classification of Brunauer, Deming, Deming, and Teller (BDDT) are present in all the isotherms of the AC sequence [48]. Form I isotherms are provided with a relatively small external surface area by overwhelmingly microporous adsorbents. The near absence of mesopores and macropores within the material was further suggested. In this way, nitrogen gas physical adsorption was effectively carried out on microporous structures [49]. A small hysteresis loop of type H4 demonstrates the desorption branch, showing greater microporosity (V_{micro} between 72% and 90% of total volume in Table 2) associated with a small contribution of the mesopore and the possible occurrence of a capillary condensation phenomenon. Furthermore, the AC products were suggested to contain mostly micropores [50]. The result suggested that both ACF_2 and ACF_3 samples contained comparatively larger and smaller amounts of micropores, respectively, and that the amount of nitrogen uptake for the ACF samples increased rapidly to a relative pressure (p/p_0) of 0.2 before the plateau was reached. If the ACF_2 sample has a higher uptake of nitrogen, then the ACF_3 sample has a lower uptake of nitrogen.

Table 2 summarizes the details of the texture properties of the manufactured carbon materials. By the BET process, the basic surface area of ACF has been observed. The BET surface areas are 278.22, 313.40, 166.29, 168.13 and 205.53 $m^2 g^{-1}$, for the ACF_1, ACF_2, ACF_3, ACF_4 and ACF_5 samples, respectively. The surface area and pore volume of the ACF_1 and ACF_2 were 278.28 and 313.40 $m^2 g^{-1}$ and 0.13 and 0.15 $cm^3 g^{-1}$, respectively. These findings indicate that the surface area of the BET is increased with the decrease in the temperature of the pyrolysis. In addition, Table 2 demonstrates that when the pyrolysis duration increased, the BET surface area increase for the ACF_3, ACF_4, and ACF_5.

Fig. 4 shows SEM micrographs of the ensemble of both types of raw fiber, RF_1 and RF_2 and all type of AC ACF_1, ACF_2, ACF_3, ACF_4 and ACF_5, respectively. The disparity between RF_1 and RF_2 is the particle size that is clearly seen in this figure in the micrograph picture that the fibers are cylindrical with their non-smooth outer surface and filled with some artificial impurities (sand and dust) and residual lignin [51]. The micrographs clearly demonstrate that, since there is a clear difference in the microstructure of these ACs, the difference in granularity affects the resulting AC.

Fig. 4 shows a cross-section for ACF_1, where the microstructural observation showed that the surface area was elliptical, almost circular in shape, and ACF_1 shows a series of multicellular fibers with central voids (lumen) in each. The multicellular fibers (individual fibers) are compactly arranged to form a technical fiber whose shape is roughly cylindrical with a smaller diameter in the range of 1–7 μm, aligned and bound together by lignin, pectin and other non-cellulosic materials [51].

The surface (longitudinal direction) SEM micrograph for ACF_2 and ACF_4 is shown in Fig. 4. On the surface of both ACs, the presence of certain impurities randomly distributed is observed. The fiber structure is oriented in the direction of the fiber axis, stacked and compacted in the form of microfibers so that they appear in layers [30]. However, the SEM images showed the AC structure in the form of nanometer hills on the surface allowing active sites to be formed in order to enhance the process of adsorption (Fig. 4), the SEM images did not vary significantly between ACF_3 and

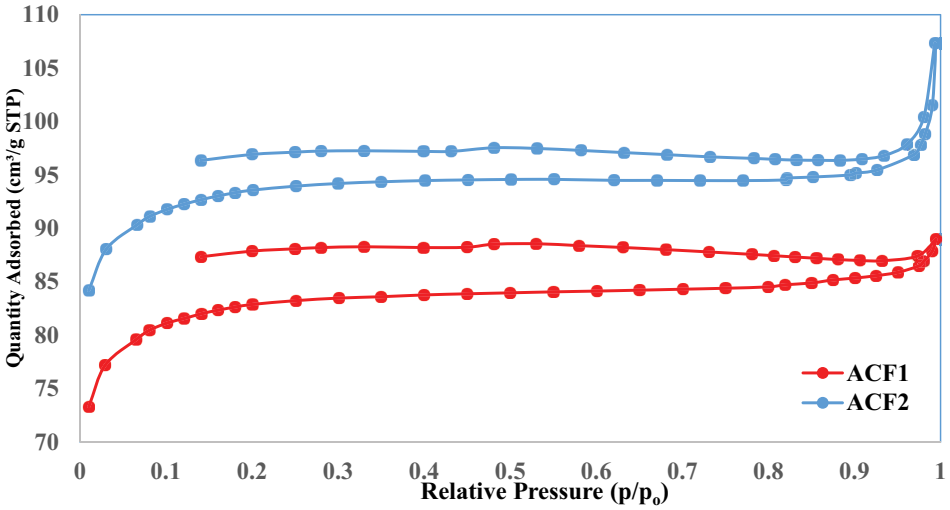

Fig. 2. Isothermal adsorption of N_2 at 77 K on activated carbon (Effect of the pyrolysis temperature on the adsorbed quantity). Pyrolysis conditions: 2 h, 250 mL/min (N_2), 5°C/min, ACF_1 600°C, ACF_2 500°C, activation condition: 600°C, 2 h, 250 mL/min (CO_2), 5°C/min.

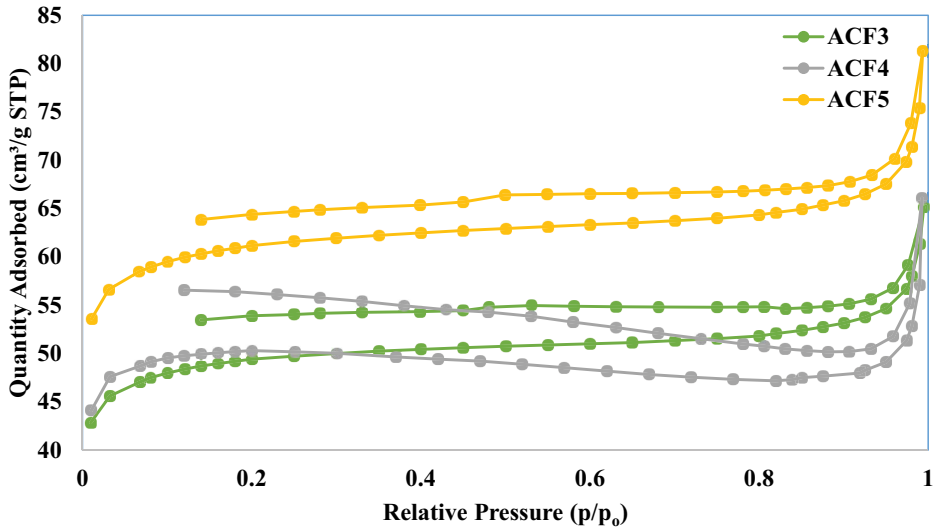

Fig. 3. Isothermal adsorption of N_2 at 77 K on activated carbon (Effect of the duration of pyrolysis on the adsorbed quantity). Pyrolysis conditions: 500°C, 250 mL/min (N_2), 5°C/min, ACF_3 1 h, ACF_4 2 h, ACF_5 3 h, activation condition: 600°C, 2 h, 250 mL/min (CO_2), 5°C/min.

ACF_5 and had almost the same morphology. The images of SEM micrographs of both raw materials and samples of AC showed that porosity and broad surface area for adsorption were produced by carbonization through pyrolysis and activation processes, thus aligned with the literature that is the objective of AC processing.

3.3. Surface chemistry characterization

Table 2 shows the material's pore size distribution data, those data indicate that due to the sharp increase in pore size distribution values for pore diameters less than 2 nm, all activated carbons are microporous materials, which indicates that most pores have existed in the range of 2–50 nm. This result is confirmed in the microporous and mesoporous volumes, Table 2 shows measured results, corresponding to 81% of the average microporosity, compared with 19% of the average mesoporosity.

D–R data of the isotherms of nitrogen adsorption of all AC are shown in Table 2. The texture parameters of the D-R isothermal equilibrium model are summarized in Table 2. The micropore size (L) of the samples ACF_1, ACF_2, ACF_3, ACF_4 and ACF_5 was 0.88, 0.77, 1.11, 0.64, 1.03 nm and the mean activation energy was 24 kJ mol^{-1} corresponding to chemisorption.

The significance of pH_{zpc} on a given AC surface is that the AC surface is positively charged when the pH is lower than the pH_{zpc} value (attracting anions). In comparison, the

Table 2
Textural and chemical properties of ACF_1, ACF_2, ACF_3, ACF_4 and ACF_5

Properties	Methods	ACF_1	ACF_2	ACF_3	ACF_4	ACF_5
Characteristics of activated carbon						
Burn-off (%)		82.38 600°C, 2 h (250 μm < D < 500 μm)	95.73 500°C, 2 h (250 μm < D < 500 μm)	93.70 500°C, 1 h (45 μm < D < 125 μm)	93.54 500°C, 2 h (45 μm < D < 125 μm)	92.96 500°C, 3 h (45 μm < D < 125 μm)
S_{BET} ($m^2\ g^{-1}$)	BET	278.22	313.40	166.29	168.13	205.53
V_T ($cm^3\ g^{-1}$)	Single point adsorption	0.13	0.15	0.09	0.08	0.11
S_{ext} ($m^2\ g^{-1}$)		36.99	37.94	29.73	13.88	35.26
S_{micro} ($m^2\ g^{-1}$)	*t*-plot	241.22	275.47	136.56	154.25	170.26
V_{micro} ($cm^3\ g^{-1}$)		0.11	0.13	0.06	0.07	0.08
V_{meso} ($cm^3\ g^{-1}$)	$V_T - V_{micro}$	0.02	0.02	0.02	0.01	0.03
S_{micro}/S_{BET} (%)		0.87	0.88	0.82	0.92	0.83
S_{ext}/S_{BET} (%)	Percentage	0.13	0.12	0.18	0.08	0.17
V_{micro}/V_T (%)		0.84	0.85	0.72	0.90	0.73
V_{meso}/V_T (%)		0.16	0.15	0.28	0.10	0.27
D_p (nm)	$4V_T/S_{BET}$	1.92	2.11	1.89	1.93	2.10
W_0 ($cm^3\ g^{-1}$)		0.11	0.12	0.07	0.07	0.08
L (nm)	D–R plot	0.88	0.77	1.11	0.64	1.03
E_0 (kJ mol^{-1})		23.64	25.43	21.11	28.19	21.85
pH_{zpc}		8.3	8.1	8.3	8.5	8
Functional groups						
$V_{carboxylic}$ (meq g^{-1})		0.077	0.107	0.119	0.095	0.107
$V_{lactone}$ (meq g^{-1})		0.140	0.082	0.079	0.079	0.044
$V_{phenolic}$ (meq g^{-1})	Boehm titration	1.408	1.161	1.552	1.825	1.449
V_{acidic} (meq g^{-1})		1.625	1.350	1.750	2.000	1.600
V_{basic} (meq g^{-1})		1.509	0.878	1.317	0.987	1.070

surface is negatively charged above pH_{zpc} (attracting cations/repelling anions). The pH_{zpc} of ACs of ACF_1, ACF_2, ACF_3, ACF_4 and ACF_5 samples were found to be 8.3, 8.1, 8.3, 8.5 and 8.0, respectively (Table 2). The pH of the solution when the ACs are added was 9.2, 9.7, 9.9, 9.7 and 9.5, respectively. As a result, the pH_{zpc} of activated carbon was lower than the pH solution, indicating that the AC surface was rich in negative charges. As a result, any sample in a slightly basic solution can be used to remove cationic contaminants.

The functional groups on the surface of each AC were calculated by the Boehm titration (Table 2). The predominance of the acidic characteristics of the carboxyl, lactone, and phenolic functional groups was shown in the results described in Table 2. The AC obtained in general has a strong acidic character, which is primarily due to the large number of groups of phenolic functions.

Fig. 5 for raw fibers and ACF samples displays the FTIR spectra, respectively. The aim of the FTIR spectroscopy investigation was to classify the AC functional groups. It should be noted that similar results from FTIR spectroscopy have been reported in the literature [52,53]. The absorption band detected in both types of raw fiber RF_1, RF_2, between 3,524 and 3,300 cm^{-1} was assigned to the hydroxyl (OH) group [46]. The presence of the OH group was due to the adsorbed moisture content, cellulose and hemicelluloses in raw fiber [54]. And the peak observed at 2,924 cm^{-1} was allocated to the cellulose CH groups. The intensity of these RF (raw fiber) absorption bands was comparatively higher compared with that of ACF. The reduction in the intensity of this ACF peak was due to the vaporization of moisture during carbonization and activation [55].

Both samples, on the other hand, have the same peaks found. The absorption bands at 1,619 and 1,419 cm^{-1} were similar to (C=C) aromatic ring bonding and C–H alkene functional groups, respectively [56]. The bands about 1,321 and 1,109 cm^{-1} were assigned to C=C–H in-plane bending (C–H deformation) and C–O ether bond stretching, respectively [57]. The peak around 1,030 cm^{-1} is attributed to the C–O–C stretching vibration in the pyranose skeleton ring, the small peaks occurring in a replacement period between 760 and 600 cm^{-1} C–H deformation were possibly due to the presence of aromatic C–H in the date palm fiber and ACF's aromatic C–H out of plane bend [58].

After the carbonization and activation processes, the produced ACF samples showed different FTIR spectra from the RF fiber. While various conditions of pyrolysis have

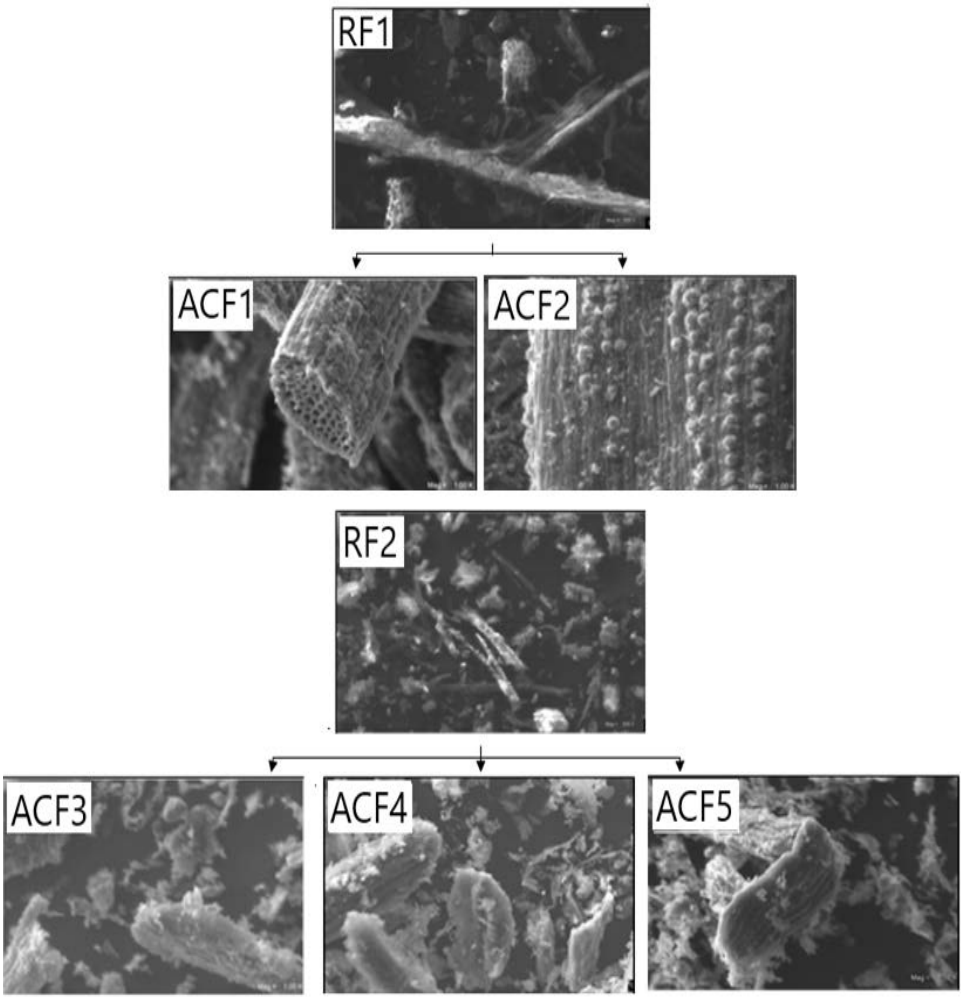

Fig. 4. Scanning electron microscopy micrographs of RF_1 and RF_2 raw fibers and ACF_1, RF_2, ACF_3, ACF_4 and ACF_5 activated carbon.

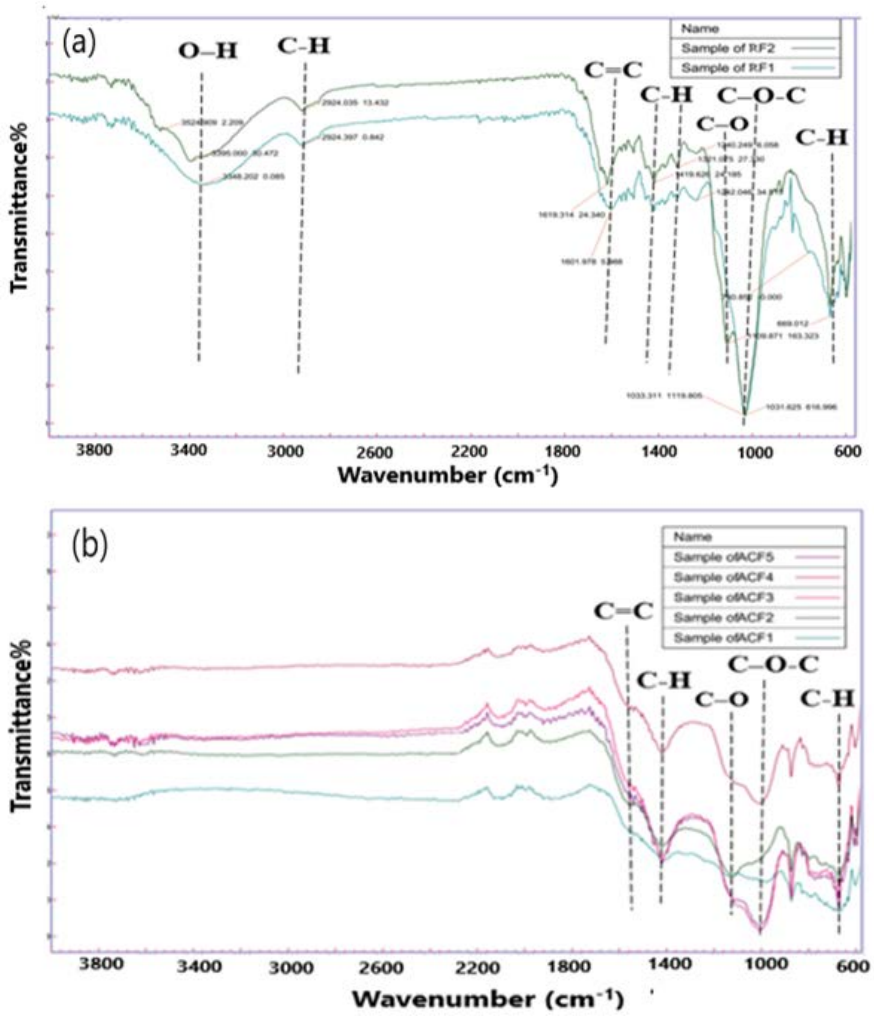

Fig. 5. (a) FT-IR spectra for RF_1 and RF_2 raw fibers and (b) the FT-IR spectra for ACF_1, ACF_2, ACF_3, ACF_4 and ACF_5 activated carbon.

been treated with the samples, it can be seen from Fig. 5 that, at most wavelengths, all ACs have similar absorption bands, suggesting their possession of similar functional groups other than ACF_1, where there is a small difference at about one peak.

The intensity of the beginning (transmittance %) of the ACF's is lower than we had in RF's, where we note that the intensity of the OH stretching and cellulose C–H groups disappeared due to CO_2 activation that enabled the functional oxygen group to be removed [58], and we also observed that in terms of transmittance the other peaks were decreased. The ACs ACF_3, ACF_4 and ACF_5 that were prepared from RF_2 were found to generally have relatively strong absorption bands than the ACFs prepared from RF_1.

3.4. Adsorption isotherm

The effects of initial phenol concentrations on the removal of phenols have been studied and shown in Fig. 6, and showed their percentages in Fig. 7. Experiments were performed at varying initial phenol concentrations of 20–100 mg L^{-1}, 0.04 g L^{-1} of ACF and 600 rpm of agitation at 25°C. As can be shown, when the initial phenol concentration increased from 20 to 100 mg L^{-1}, removal of phenol of ACF_1, ACF_2, ACF_3, ACF_4 and ACF_5 decreased from 42.98%, 42.38%, 68.84%, 38.93% and 57.20% to 40.98%, 34.23%, 47.84%, 36.63% and 43.97%, respectively, and the uptake capacity increased from 2.11, 2.12, 3.44, 1.95, and 2.86 mg g^{-1} to 10.24, 8.56, 11.96, 9.16, and 10.99 mg g^{-1}, respectively, after adsorption time of 180 min. The increase in the amount of adsorbed phenol at equilibrium (q_e) with an increase in phenol concentration is attributable to a higher availability of phenol molecules in the adsorption solution and a higher interaction between the adsorbent and the adsorbate at a higher phenol concentration, which could be due to an increase in the driving force of the phenol molecules towards the adsorbent [43].

The fact that all adsorbents have a limited number of active sites, which would have been saturated above a certain concentration, can explain the decrease in the percentage removal. The classification of adsorption isotherms of phenol is L4-curve (the normal), according to Giles et al. [60], this class implies that the slope gradually falls with an increase in concentration and with the gradual covering

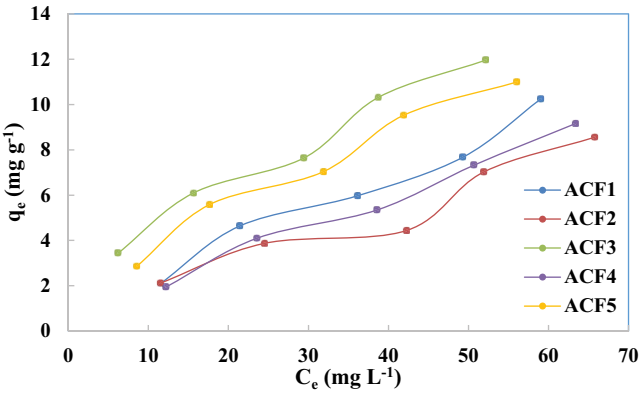

Fig. 6. Effect of the initial concentration of phenol on the adsorption capacity onto ACF_1, ACF_2, ACF_3, ACF_4 and ACF_5 activated carbon at 25°C.

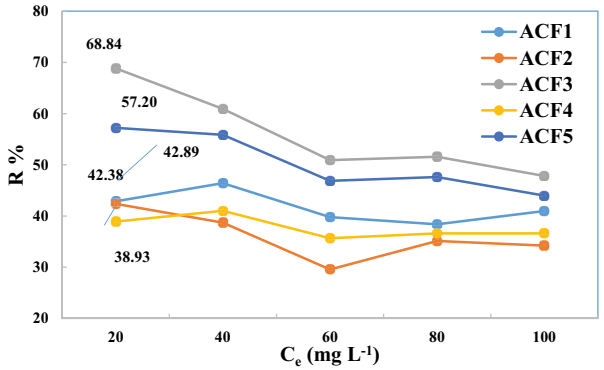

Fig. 7. Effect of the initial concentration of phenol on the percentage removal of adsorption.

of the surface it becomes more difficult to find vacant sites. ACF_2 was found to have the highest phenol adsorption capacity, followed by ACF_4, ACF_1, ACF_5 and ACF_3 for the concentration range tested in this study, with the pores diameter calculated in this study for ACF_1, ACF_2, ACF_3, ACF_4 and ACF_5 being 1.92, 2.11, 1.89, 1.93, and 2.10 nm, respectively. The difference in this value for these adsorbents and the higher specific surface area (313.40 m^2/g) explains the higher adsorption capacities of phenol for ACF_2 compared with the other ACs. We also noted that the largest removal of phenol was in the low concentrations.

In order to research the adsorption activity at various phenol concentrations, Langmuir and Freundlich isothermal models were used. The linearized phenol isotherms from Langmuir and Freundlich are shown in Fig. 8 as well as Fig. 9. Two isothermal models were used to obtain results and regression coefficients, and the results were consistent with the experimental evidence (Table 3). Parameters such as the K_L, the adsorption equilibrium constant, which is related to adsorption free energy and corresponds to the affinity between the adsorbent surface and the adsorbate, are given by the Langmuir model. As well as the maximum adsorption capacity (q_{max}) that is combined with the amount of phenol adsorbed to complete a monolayer, full coverage is

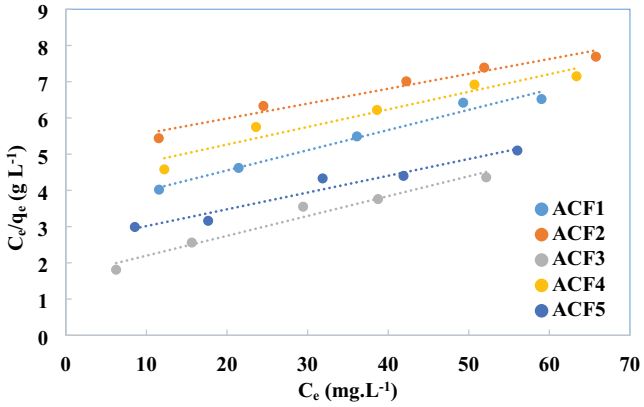

Fig. 8. Langmuir plot for the adsorption of phenol onto ACF_1, ACF_2, ACF_3, ACF_4 and ACF_5 activated carbon at 25°C.

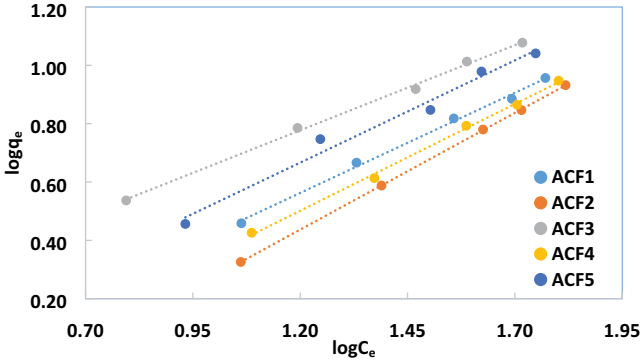

Fig. 9. Freundlich plot for the adsorption of phenol onto ACF_1, ACF_2, ACF_3, ACF_4 and ACF_5 activated carbon at 25°C.

achieved when all existing sites have been filled. The values of ACF_1, ACF_2, ACF_3, ACF_4, and ACF_5 in the q_{max} Langmuir model were found to be 21.74, 31.75, 15.29, 23.26 and 18.38 mg g^{-1}, respectively. In the present experiment, factors (R_L) were found to be 0.34, 0.54, 0.23, 0.62, and 0.35. All the R_L values indicate that the adsorption was favorable.

In general, the Freundlich n-value of an effective adsorbent is between 1 and 10. It was found that the value of n was 1.12, 1.31, 1.74, 1.10 and 1.43, respectively. The values of $n > 1$ represent favorable adsorption conditions, indicating the favorable adsorption of phenol onto ACF's.

Table 3 shows that the regression coefficient (R^2, χ^2 and $F_{error\%}$ obtained from the isothermal models of Langmuir and Freundlich showed values of ($R^2 > 0.9806$, $\chi^2 < 0.22$ and $F_{error\%}$) < 8.19) and ($R^2 > 0.9678$, $\chi^2 < 0.35$ and $F_{error\%} < 9.28$). These results indicated that both the Langmuir and Freundlich isotherm models can adequately describe the adsorption data. The applicability of the two isotherm models to the investigated systems implies that both monolayer adsorption (i.e., only a limited number of surface sites are adsorbing sites for the phenol molecule) and heterogeneous surface conditions exist under the experimental conditions studied.

4. Conclusion

This study shows that date palm fiber can be effectively utilized as a raw material for ACF production. The

Table 3
Parameters of the Langmuir and Freundlich adsorption isotherm models for ACF_1, ACF_2, ACF_3, ACF_4 and ACF_5

Adsorbent	ACF_1	ACF_2	ACF_3	ACF_4	ACF_5
			Langmuir isotherm		
q_{max} (mg g^{-1})	21.74	31.75	15.29	23.26	18.38
K_L (L mg^{-1})	0.020	0.01	0.03	0.01	0.02
R_L	0.34	0.54	0.23	0.62	0.35
R^2	0.9806	0.9869	0.9897	0.9939	0.9969
χ^2	0.22	0.22	0.07	0.05	0.02
$F_{error\%}$	8.19	7.75	4.13	4.71	2.68
			Freundlich isotherm		
K_F [(mg g^{-1})(L $mg^{-1})^{1/n}$]	0.26	0.32	1.20	0.21	0.67
N	1.12	1.31	1.74	1.10	1.43
R^2	0.9678	0.9692	0.9790	0.9873	0.9808
χ^2	0.18	0.35	0.11	0.08	0.13
$F_{error\%}$	9.28	9.17	4.28	5.30	5.75

highest burn-off was 95.73 wt% for the ACF_2. From the N_2 adsorption–desorption isotherm at 77 K, we found a clear different structures of samples, while the higher amount of nitrogen adsorbed is for ACF_2 sample, and with BET surface area 313.40 m^2 g^{-1}, and pores diameter 1.93 nm. Well-developed micropore structures with different morphologies of palm date fiber after activation processes were found by the SEM image, which is compatible with the pore size distribution curve. The D-R isotherm showed that the adsorption type is chemisorption, the pH_{zpc} and Boehm titration have also shown the richness in negative charges and acidic characteristics, respectively, of ACs. FTIR study of both RF's and ACF's was carried out and found different functional groups. The removal of phenol from aqueous solution using ACF's prepared from date palm fiber has been investigated quite effectively. The maximum adsorption capacity of phenol onto ACF's was observed as high as 31.75 mg g^{-1} of ACF_4, it should also be noted that the samples showed that the highest percentage of adsorption was at low phenol concentration. The equilibrium adsorption data were satisfactorily fitted to Langmuir and Freundlich isotherms. As concluded overall, ACF_2 is the one that has the most adsorption value in the gas phase, unlike the liquid phase, while ACF_4 has the largest adsorption value in the liquid phases over the gas phase. ACF_2 is larger in the size of the grains and the surface area of ACF_3, unlike the pore diameter, ACF_4 has the largest pores in diameter, all these confirm that the structural properties have an effect on the selectivity of the adsorption phases.

References

[1] Q.-S. Liu, T. Zheng, P. Wang, J.-P. Jiang, N. Li, Adsorption isotherm, kinetic and mechanism studies of some substituted phenols on AC fibers, Chem. Eng. J., 157 (2010) 348–356.

[2] Y. Li, X. Hu, X. Liu, Y. Zhang, Q. Zhao, P. Ning, S. Tian, Adsorption behavior of phenol by reversible surfactant-modified montmorillonite: mechanism, thermodynamics, and regeneration, Chem. Eng. J., 334 (2018) 1214–1221.

[3] M.H. El-Naas, S. Al-Zuhair, M.A. Alhaija, Removal of phenol from petroleum refinery wastewater through adsorption on date-pit AC, Chem. Eng. J., 162 (2010) 997–1005.

[4] J. Rouquerol, F. Rouquerol, P. Llewellyn, G. Maurin, K.S.W. Sing, Adsorption by Powders and Porous Solids: Principles, Methodology and Applications, Academic Press, Elsevier, Paris, 2013.

[5] M. Alshabanat, G. Alsenani, R. Almufarij, Removal of crystal violet dye from aqueous solutions onto date palm fiber by adsorption technique, J. Chem., 2013 (2013) 210239.

[6] H. Marsh, F.R. Reinoso, Activated Carbon, Elsevier, 2006.

[7] R.C. Bansal, M. Goyal, AC Adsorption, Activated Carbon Adsorption, CRC Press, Taylor & Francis, London, 2005.

[8] G. Crini, E. Lichtfouse, L.D. Wilson, N. Morin-Crini, Adsorption-oriented processes using conventional and non-conventional adsorbents for wastewater treatment, Green Adsorbents Pollut. Removal, 18 (2018) 23–71.

[9] R.I. Yousef, B. El-Eswed, H. Ala'a, Adsorption characteristics of natural zeolites as solid adsorbents for phenol removal from aqueous solutions: kinetics, mechanism, and thermodynamics studies, Chem. Eng. J., 171 (2011) 1143–1149.

[10] R. Fang, H. Huang, J. Ji, M. He, Q. Feng, Y. Zhan, D.Y.C. Leung, Efficient MnOx supported on coconut shell AC for catalytic oxidation of indoor formaldehyde at room temperature, Chem. Eng. J., 334 (2018) 2050–2057.

[11] E. Díaz, A.F. Mohedano, L. Calvo, M.A. Gilarranz, J.A. Casas, J.J. Rodríguez, Hydrogenation of phenol in aqueous phase with palladium on AC catalysts, Chem. Eng. J., 131 (2007) 65–71.

[12] M. Yu, Y. Han, J. Li, L. Wang, CO_2-activated porous carbon derived from cattail biomass for removal of malachite green dye and application as supercapacitors, Chem. Eng. J., 317 (2017) 493–502.

[13] L.A. Rodrigues, M.L.C.P. da Silva, M.O. Alvarez-Mendes, A. dos Reis Coutinho, G.P. Thim, Phenol removal from aqueous solution by AC produced from avocado kernel seeds, Chem. Eng. J., 174 (2011) 49–57.

[14] P. Girods, A. Dufour, V. Fierro, Y. Rogaume, C. Rogaume, A. Zoulalian, A. Celzard, ACs prepared from wood particleboard wastes: characterisation and phenol adsorption capacities, J. Hazard. Mater., 166 (2009) 491–501.

[15] F. Boudrahem, F. Aissani-Benissad, H. Aït-Amar, Batch sorption dynamics and equilibrium for the removal of lead ions from aqueous phase using AC developed from coffee residue activated with zinc chloride, J. Environ. Manage., 90 (2009) 3031–3039.

[16] R.U. Edgehill, G.Q. Lu, Adsorption characteristics of carbonized bark for phenol and pentachlorophenol, J. Chem. Technol. Biotechnol., 71 (1998) 27–34.

[17] B. Petrova, T. Budinova, B. Tsyntsarski, V. Kochkodan, Z. Shkavro, N. Petrov, Removal of aromatic hydrocarbons from water by AC from apricot stones, Chem. Eng. J., 165 (2010) 258–264.
[18] M.L. Sekirifa, M. Hadj-Mahammed, S. Pallier, L. Baameur, D. Richard, A.H. Al-Dujaili, Preparation and characterization of an AC from a date stones variety by physical activation with carbon dioxide, J. Anal. Appl. Pyrolysis, 99 (2013) 155–160.
[19] M.L. Sekirifa, S. Pallier, M. Hadj-Mahammed, D. Richard, L. Baameur, A.H. Al-Dujaili, Measurement of the performance of an agricultural residue-based AC aiming at the removal of 4-chlophenol from aqueous solutions, Energy Procedia, 36 (2013) 94–103.
[20] M. Abdulkarim, F.A. Al-Rub, Adsorption of lead ions from aqueous solution onto AC and chemically-modified AC prepared from date pits, Adsorpt. Sci. Technol., 22 (2004) 119–134.
[21] M. Belhachemi, Z. Belala, D. Lahcene, F. Addoun, Adsorption of phenol and dye from aqueous solution using chemically modified date pits ACs, Desal. Wat. Treat., 7 (2009) 182–190.
[22] M.T. Amin, A.A. Alazba, M. Shafiq, Adsorption of copper (Cu^{2+}) from aqueous solution using date palm trunk fibre: isotherms and kinetics, Desal. Wat. Treat., 57 (2016) 22454–22466.
[23] S.M. Yakout, G.S. El-Deen, Characterization of AC prepared by phosphoric acid activation of olive stones, Arabian J. Chem., 9 (2016) S1155–S1162.
[24] C.A. Garcia, J.C.G. Moraes, E.M. Nogami, E. Lenzi, W.F. Costa, V.C. Almeida, Preparation and characterization of AC from a new raw lignocellulosic material: Flamboyant (*Delonix regia*) pods, J. Environ. Manage., 92 (2011) 178–184.
[25] K.S.K. Reddy, A. Al Shoaibi, C. Srinivasakannan, A comparison of microstructure and adsorption characteristics of ACs by CO_2 and H_3PO_4 activation from date palm pits, New Carbon Mater., 27 (2012) 344–351.
[26] Y.-b. Tang, Q. Liu, F.-y. Chen, Preparation and characterization of AC from waste ramulus mori, Chem. Eng. J., 203 (2012) 19–24.
[27] T. Zhang, W.P. Walawender, L. Fan, M. Fan, D. Daugaard, R. Brown, Preparation of AC from forest and agricultural residues through CO_2 activation, Chem. Eng. J., 105 (2004) 53–59.
[28] B. Sajjadi, W.Y. Chen, N.O. Egiebora, A comprehensive review on physical activation of biochar for energy and environmental application, Rev. Chem. Eng., 35 (2018) 1–42.
[29] N. Bouguedoura, M. Bennaceur, S. Babahani, S. E. Benziouche, Date Palm Status and Perspective in Algeria, In: Date Palm Genetic Resources and Utilization, Springer, Netherlands, 2015, pp. 125–168.
[30] H. Boumediri, A. Bezazi, G.G. Del Pino, A. Haddad, F. Scarpa, A. Dufresne, Extraction and characterization of vascular bundle and fiber strand from date palm rachis as potential bio-reinforcement in composite, Carbohydr. Polym., 222 (2019) 114997.
[31] F.M. Al-Oqla, O.Y. Alothman, M. Jawaid, S.M. Sapuan, M.H. Es-Saheb, Processing and Properties of Date Palm Fibers and Its Composites, In Biomass and Bioenergy, Springer, Netherlands, 2014, pp. 1–25.
[32] M. Paradis, Rapport sur le commerce extérieur des dattes, 2017.
[33] S. Brunauer, P.H. Emmett, E. Teller, Adsorption of gases in multimolecular layers, J. Am. Chem. Soc., 60 (1938) 309–319.
[34] K.S.W. Sing, Reporting physisorption data for gas/solid systems with special reference to the determination of surface area and porosity (Recommendations 1984), Pure Appl. Chem., 57 (1985) 603–619.
[35] N.P. Dubinin, Work of Soviet biologists: theoretical genetics, Science, 105 (1947) 109–112.
[36] Y. El Maguana, N. Elhadiri, M. Bouchdoug, M. Benchanaa, Study of the influence of some factors on the preparation of AC from walnut cake using the fractional factorial design, J. Environ. Chem. Eng., 6 (2018) 1093–1099.
[37] F. Boudrahem, I. Yahiaoui, S. Saidi, K. Yahiaoui, L. Kaabache, M. Zennache, F. Aissani-Benissad, Adsorption of pharmaceutical residues on adsorbents prepared from olive stones using mixture design of experiments model, Water Sci. Technol., 80 (2019) 1–12.
[38] H.P. Boehm, Chemical Identification of Surface Groups, In: D.D. Eley, H. Pines, P.B. Weisz, Eds., Advances in Catalysis, Academic Press, Vol. 16, 1966, pp. 179–274.
[39] D. Prahas, Y. Kartika, N. Indraswati, S. Ismadji, AC from jackfruit peel waste by H_3PO_4 chemical activation: pore structure and surface chemistry characterization, Chem. Eng. J., 140 (2008) 32–42.
[40] P. González-García, AC from lignocellulosics precursors: a review of the synthesis methods, characterization techniques and applications, Renewable Sustainable Energy Rev., 82 (2018) 1393–1414.
[41] M.J. Ahmed, Preparation of ACs from date (*Phoenix dactylifera L.*) palm stones and application for wastewater treatments: review, Process Saf. Environ. Protect., 102 (2016) 168–182.
[42] K.Y. Foo, B.H. Hameed, An overview of dye removal via AC adsorption process, Desal. Wat. Treat., 19 (2010) 255–274.
[43] S. Afshina, Y. Rashtbaria, M. Shirmardic, M. Vosoughib, A. Hamzehzadeha, Adsorption of Basic Violet 16 dye from aqueous solution onto mucilaginous seeds of Salvia sclarea: kinetics and isotherms studies, Desal. Wat. Treat., 161 (2019) 365–375.
[44] A.M.A. Al-Haidary, F.H.H. Zanganah, S.R.F. Al-Azawi, F.I. Khalili, A.H. Al-Dujaili, A study on using date palm fibers and leaf base of palm as adsorbents for Pb (II) ions from its aqueous solution, Water Air Soil Pollut., 214 (2011) 73–82.
[45] A. El Hanandeha, Z. Mahdi, M.S. Imtiaz, Modelling of the adsorption of Pb, Cu and Ni ions from single and multi-component aqueous solutions by date seed derived biochar: comparison of six machine learning approaches. Environ. Res., 192 (2021) 110338.
[46] M.C. Silva, L. Spessato, T.L. Silva, G.K.P. Lopes, H.G. Zanella, J.T.C. Yokoyama, A.L. Cazetta, V.C. Almeida, H_3PO_4–AC fibers of high surface area from banana tree pseudo-stem fibers: adsorption studies of methylene blue dye in batch and fixed bed systems, J. Mol. Liq., 2020 (2020) 114771.
[47] C.H. Ooi, W.K. Cheah, Y.L. Sim, S.Y. Pung, F.Y. Yeoh, Conversion and characterization of AC fiber derived from palm empty fruit bunch waste and its kinetic study on urea adsorption, J. Environ. Manage., 197 (2017) 199–205.
[48] S. Brunauer, L.S. Deming, W.E. Deming, E. Teller, On a theory of the van der Waals adsorption of gases, J. Am. Chem. Soc., 62 (1940) 1723–1732.
[49] A. Aworn, P. Thiravetyan, W. Nakbanpote, Preparation and characteristics of agricultural waste AC by physical activation having micro-and mesopores, J. Anal. Appl. Pyrolysis, 82 (2008) 279–285.
[50] O. Belaid, A.A. Bebba, M.L. Sekirifa, L. Baameur, A.H. Al-Dujaili, Preparation and characterization of chemically ACs from different varieties of date stones, Desal. Wat. Treat., 65 (2017) 267–273.
[51] M. Alhijazi, Q. Zeeshan, M. Safaei, M. Asmael, Z. Qin, Recent developments in palm fibers composites: a review, J. Polym. Environ., 28 (2020) 3029–3054.
[52] E. Galiwango, N.S.A. Rahman, A.H. Al-Marzouqi, M.M. Abu-Omar, A.A. Khaleel, Isolation and characterization of cellulose and α-cellulose from date palm biomass waste, Heliyon, 5 (2019) e02937.
[53] K. Riahi, B.B. Thayer, A.B. Mammou, A.B. Ammar, M.H. Jaafoura, Biosorption characteristics of phosphates from aqueous solution onto *Phoenix dactylifera L.* date palm fibers, J. Hazard. Mater., 170 (2009) 511–519.
[54] H. Yang, R. Yan, H. Chen, D.H. Lee, C. Zheng, Characteristics of hemicellulose, cellulose and lignin pyrolysis, Fuel, 86 (2007) 1781–1788.
[55] M. Keiluweit, P.S. Nico, M.G. Johnson, M. Kleber, Dynamic molecular structure of plant biomass-derived black carbon (biochar), Environ. Sci. Technol., 44 (2010) 1247–1253.
[56] J. Coates, Interpretation of Infrared Spectra, a Practical Approach. Encyclopedia of Analytical Chemistry: Applications, Theory and Instrumentation, Wiley, New York, 2006.

[57] A.K. Mohammed, A.A. Abdulhassan, W.Y. Al-Meshhdany, Biosorption of chromium ions from aqueous solutions by using date palm fibers, Iraqi J. Biotechnol., 16 (2017) 8–14.
[58] F. Benstoem, G. Becker, F. Benstoem, G. Becker, J. Firk, M. Kaless, D. Wuest, J. Pinnekamp, A. Kruse, Elimination of micropollutants by AC produced from fibers taken from wastewater screenings using hydrothermal carbonization, J. Environ. Manage., 211 (2018) 278–286.
[59] Q. Abbas, M. Mirzaeian, A.A. Ogwu, M. Mazur, D. Gibson, Effect of physical activation/surface functional groups on wettability and electrochemical performance of carbon/AC aerogels based electrode materials for electrochemical capacitors, Int. J. Hydrogen Energy, 45 (2020) 13586–13595.
[60] C.H. Giles, D. Smith, A. Huitson, A general treatment and classification of the solute adsorption isotherm. I. Theoretical, J. Colloid Interface Sci., 47 (1974) 755–765.